OPTICAL IMAGING OF CELL CYCLE-DRIVEN TUMOR HETEROGENEITY

By

Tiffany Marie Heaster

Thesis
Submitted to the Faculty of the
School of Engineering of Vanderbilt University
in partial fulfillment of the requirements
for the degree of

MASTER OF SCIENCE
in
Biomedical Engineering

May, 2016

Nashville, Tennessee

Approved:

Melissa C. Skala, Ph.D.

Frederick R. Haselton, Ph.D.

ACKNOWLEDGEMENTS

TABLE OF CONTENTS

Chapter

LIST OF TABLES

LIST OF FIGURES

CHAPTER I

INTRODUCTION

Tumor Heterogeneity and Treatment Resistance

One of the greatest limitations in the treatment of cancer is development of resistance to the therapeutic effects of common chemotherapies. Though rates of recurrence vary dependent on cancer type, there is a high prevalence of tumor recurrence in cancer patients universally. Notably, identification of sources of treatment resistance has become a primary focus of ongoing cancer research. Several factors contributing to resistance have been established, however, these mechanisms and the significance of each in driving resistance are not thoroughly understood [1]. Primarily, genetic mutations have been recognized as having implications in treatment response, affecting cellular sensitivity to drug. Further studies have suggested functional differences of cells comprising the tumor, and those occupying the surrounding tissue, play a role in modulating treatment efficacy. It is necessary to develop a fundamental understanding of where resistant cells originate and the underlying mechanisms dictating their function [3]. Establishment of a technology to study and characterize the progression of cancer cells from drug-responsive to drug-resistant would inform treatment decisions to target responsive pathways, which would greatly enhance patient treatment response and have implications on both patient well-being and burden of adverse treatment effects and cost.

Tumor heterogeneity contributes largely to lack of cellular response to standard chemotherapy. Subpopulations of tumor cells can be identified within the bulk mass, each exhibiting unique function. Upon administration of first line therapy, the majority of cells respond

to and are eliminated from the treatment site [28]. However, select subpopulations can evade treatment by operating under mechanisms dissimilar to the bulk populations, of which the drug does not target. The residual cells can then proceed to repopulate the previously diseased region, occupied by an abundance of drug-resistant cells [1]. Subsequent treatment regimens become ineffective, allowing survival and spread of the tumor. There is a deficiency in the understanding of molecular mechanisms regulating the heterogeneous nature of cells and the consequent treatment response. Furthermore, current methods applied to characterize heterogeneity within tumors involve highly invasive protocols, disrupting the environmental dynamics influencing heterogeneous development. Flow cytometry is the current gold standard for sorting heterogeneous cell samples into their respective populations, but presents limitations to preserving the natural tumor cell environment and requires prior knowledge of sample content for label selection [16]. Also, this technique provides minimal functional information, which is vital to detect and comprehend sources of heterogeneity. Thus, there is a need to develop label-free tools to image heterogeneous populations within intact tumor samples and simultaneously provide a functional metric correlated to cell-specific heterogeneity.

Cell Cycle Activity as a Source of Heterogeneity

Overall, the cell cycle is characterized by series of complex processes involved in governing cell generation and maintenance. Cell cycle mechanisms are inherently designed to prepare the cell for proliferation events, sustain the cellular environment despite lack of nutrients, and eliminate defective cells. Generally, proliferation can be defined as a state in which cells are systematically progressing through the stages of the cell cycle [16]. This encompasses periods of regulated cell development and reproduction. Upon influence from environment changes, cellular

signaling can induce cellular transition to exit the cell cycle and occupy a phase termed quiescence. Quiescence is characterized by a lapse in cell production despite maintaining viability [16]. Notably, cells entering a state of quiescence often only temporarily occupy this phase, indicating the possibility of re-entry into the cell cycle for continued cell growth and development. Furthermore, cells can undergo regulated death events referred to as apoptosis. Each of the aforementioned cellular activity states is associated with characteristic shifts in metabolic activity, introducing both functional and metabolic heterogeneity to biological systems [16, 25]. Cancer cells can exploit cell cycle activity by regulating activation and inhibition of the cell cycle. Cellular response to administered treatment can fluctuate to relative the position in the cell cycle [27]. This results in cell populations conferring resistance to standard chemotherapies likely due to variations in cellular function dependent on cell cycle status. Therefore, cell cycle status and its environmental influence should be addressed when considering sources of tumor heterogeneity and associated challenges [26].

Metabolism as a Marker of Cell Cycle Activity

Reduced nicotinamide adenine dinucleotide (NADH) and flavin adenine dinucleotide (FAD) are intracellular coenzymes that have a significant functional role in biological processes at the cellular level [1]. Both serve as essential components in reactions involved in key metabolic pathways, as either reactants or byproducts. Specifically, presence of NADH can directly regulate functionality of mitochondria and intracellular energy production, as well as factors influencing cellular maturity and death. NADH involvement in glycolysis reveals significant information regarding metabolic activity in varied physiological states. Notably, cells under abnormal physiological conditions utilize glycolytic processes to supply ATP, resulting in greater production

of NADH. This allows characterization of the relationship between glycolytic rates and pathophysiology through observation of NADH concentration [1]. Additionally, studies have suggested that a similar relationship can be established between glucose uptake and NADH concentration, providing supplementary metrics to cellular function. Similarly, FAD production has been identified to have direct correlation with eukaryotic cellular respiration processes, such as oxidative phosphorylation [2]. The citric acid cycle functions to co-regulate cellular metabolism, requiring both NADH and FAD as contributors. Fluctuations in NADH and FAD concentrations can be representative of overall respiratory chain response to external influences [3]. Monitoring changes in cellular function using NADH and FAD biomarkers is not limited to simply metabolic processes. Often, mechanisms of metabolism can be associated with altered states within the cellular environment, such as oxidative stress levels. Overall, these metabolic coenzymes allow comprehensive visualization of cellular activity as well as influencing factors.

Metabolism has been identified as a principal regulator of global cellular activity and transition between cell cycle phases. Accordingly, modulation of metabolic products has implications in determining cellular function and cell cycle status. Specifically, in a leukemic cell model, cells actively proliferating exhibit stable progression through each phase of the cell cycle, which can be indicated by upregulation of oxidative metabolite (e.g. Acetyl-CoA) production [17]. This correlates with increased FAD generation, characteristic of active energy production via oxidative phosphorylation [18, 19]. Similarly, previous studies have suggested variation in intracellular NADH levels are associated with changes in growth rate. Upon cellular transition into a quiescent state, there is an observable decrease in NADH production associated with a reduced reliance on oxidative phosphorylation for energy production [19]. Furthermore, damage induced

by oxidative stress signals activity within different pathways involved in ATP and NADH production, as well as FAD consumption [2]. Increasing oxidative stress levels, along with other damage-causing factors, are responsible for mitochondrial initiation of cell death. Consequently, mitochondria-driven apoptosis will also produce varied NADH and FAD concentrations [14]. Therefore, concentrations of NADH and FAD should ideally correlate with changes in cell development, establishing metabolic activity changes as valid biomarkers for cell cycle status.

Optical Imaging of Cellular Metabolism

Metabolic coenzymes NADH and FAD demonstrate strong autofluorescent properties allowing ease of observation via fluorescence imaging techniques [3]. Autofluorescence of NADH and FAD exhibit spectral characteristics that are unique to each respective fluorophore. Excitation spectra of these molecules are well separated, with excitation maxima of 350 nm for NADH and 435 nm for FAD. Additionally, NADH and FAD exhibit a Stokes shift in their emitted signal with an emission maxima of 460 nm and 535 nm, respectively [12]. NADH has been associated with greater overall fluorescence intensity, due to higher quantum yield compared to FAD. However, the concentration of each fluorophore in a sample primarily dictates the detectability of autofluorescence. This feature allows quantification of fluorophore present from the measured autofluorescence signal and correlation to active metabolic pathways in a given sample [13]. Due to their involvement in cellular metabolism and unique fluorescence signatures, both coenzymes act as key indicators of physiological change within an organism. Utilizing its intrinsic autofluorescence, NADH concentrations can be quantified to provide early identification of abnormalities within the cellular environment [3]. Due to the stable autofluorescent properties exhibited by both, these molecules have been identified as effective metabolic biomarkers.

Supplementary information inherently associated with cellular metabolism can be probed by observing fluorescence lifetime of metabolic products. Fluorescence lifetime can be defined as the time for a molecule to relax to the ground energy state following photon absorption and excitation to a higher energy state [10]. The fluorescence lifetimes of NADH and FAD measure the protein binding activity of the respective fluorophore. Enzymatic binding of NADH and FAD can result in fluorescence lifetime variations, due to conformational changes in these molecule [7]. NADH in an unbound state exhibits partial quenching of its adenine side chain, resulting in a faster rate of fluorescence decay than in the unquenched, bound form [4]. The opposite trend is observable with FAD, with its bound form undergoing quenching and subsequently, exhibiting slower fluorescence decay. These variations in fluorescence lifetime can be correlated to environmental changes within biological samples, establishing the capacity of these molecules to serve as biomarkers.

Subsequently, other metrics of metabolism exploit NADH and FAD activity to understand intracellular mechanisms. Quantification of change in metabolic activity is frequently described using a measurement known as the redox ratio. Redox ratio examines the relative abundance of NADH and FAD per cell by calculation of the ratio of NADH intensity over FAD intensity [3, 7]. This metric provides a global assessment of intracellular metabolic activity and can be indicative of the active metabolic pathways across cell type and in response to various perturbations. For example, increased redox ratio values are suggested to correlate with amplified NADH production associated with glycolytic metabolism. Oxidative metabolism causes simultaneous consumption of NADH and FAD production, observable through relative decreases in redox ratio.

Cancerous tissue can be characterized by the response to environmental stimuli (e.g. changes in oxygen level, glucose availability) and feature expression specific to the degree of severity. This has initiated attempted analysis of potential sources for cancer development. Recently, consideration has been given to the effects of metabolic dysfunction on cancer onset. Inhibiting respiration pathways within mitochondria in conjunction with glycolysis stimulation have been shown to correlate with cancerous cell growth [4]. Additional differences can be observed in the phenotype and genetic makeup of cancerous mitochondria as opposed to normal mitochondria. Altered cellular function associated with cancer cells, specifically metabolic activity differences, are significant indicators for understanding response to physiological condition. Influence of metabolism on cancer development presents defined characteristics to allow for improved means of identification and analysis. Past pilot studies have examined levels of NADH autofluorescence between various cancer cell lines to determine that NADH concentration could function as a biomarker within all cancer types. Additionally, changes in autofluorescent signal within cancer cells have been analyzed in response to drug treatment [4-9]. Characteristic of tumor metabolism, decreases in protein bound NADH were observed in the presence of dysplasia, attributed to a transition of active metabolic pathways from oxidative phosphorylation to glycolysis. These fluctuations in protein bound NADH also correlate with severity of precancerous tissue, allowing differentiation between normal, low-grade, and high grade dysplasia [4, 6-9]. Notably, identification of early stage cancer growth has been attempted utilizing autofluorescence of both NADH and FAD concentrations to establish defined signatures from cells at each stage. Signals were found to be proportional with degree of malignancy and cytoplasmic prevalence, displaying enhanced metabolic activity in highly invasive cells with smaller cytoplasmic areas. These studies have identified metabolism as an effective measure of cancer progression.

CHAPTER II

MANUSCRIPT: OPTICAL METABOLIC IMAGING OF HETEROGENEOUS, CELL CYCLE-DRIVEN TUMOR CELL SUBPOPULATIONS

Introduction

The metabolism, drug response, and genetic expression of cells is heterogeneous within a single tumor, which affects cancer progression and response to treatment [1]. Specifically, quiescent cancer cells lack responsiveness to standard chemotherapies, introducing a major challenge to efficacy of cancer treatment [17, 25]. Quiescent populations have been suggested to largely influence tumors to enter a state of dormancy, in which the bulk mass is typically unresponsive to therapy. This results in residual cancer cell populations following treatment that drive tumor relapse. However, the mechanisms responsible for the origin of quiescent cell populations and interactions with their micro-environment are not well understood. Identifying quiescent cells within tumors could promote the development of improved therapies to target these resistant cell populations.

Flow cytometry is a standard measure of cell function, and is used to identify quiescent and resistant cancer cells in heterogeneous tumors. Flow cytometry requires labeling cells with fluorescent dyes and sorting the cells into pure populations *ex vivo*. One notable limitation of flow cytometry includes the use of these fluorescent labels, which disrupt of cell physiology [16]. Additionally, flow cytometry requires the dissociation of the sample into a single cell suspension *ex vivo*, and thus loses the spatial context of each sub-population. Characterizing heterogeneous sub-populations in intact samples would inform on cell clustering and spatial relationships with other cells in the tumor, thus providing a more complete picture of tumor heterogeneity.

8

Optical metabolic imaging (OMI) is attractive for the study of tumor heterogeneity because it is non-invasive, does not use exogenous labels, can be conducted in intact samples [7-9, 15] including *in vivo* tumors [28], achieves cellular resolution, and is sensitive to cell metabolism [2]. Cell metabolism is a sensitive measure of cell malignancy, cancer progression, and an early measure of tumor cell drug response [7-9]. Metabolic changes can be optically quantified using the distinct autofluorescent properties of the metabolic co-enzymes NAD(P)H and FAD. The fluorescence intensities of NAD(P)H and FAD can be combined into the "optical redox ratio" (fluorescence intensity of NAD(P)H / FAD), which is sensitive to the relative amounts of electron donor and acceptor in a cell. The redox ratio was established by Chance et al. [13] and has since been used for an array of applications in cancer, including studies of cancer progression, invasion, and drug response [3, 7-9, 15]. Fluorescence lifetime imaging provides a complementary measurement to the redox ratio [28], and is sensitive to the enzyme binding activities of NAD(P)H and FAD [10]. Specifically, the protein-bound NAD(P)H lifetime is significantly longer than the free NAD(P)H lifetime, due to self-quenching in the free state [7, 10, 21-23]. Conversely, FAD lifetimes are short and long in the protein-bound and free states, respectively [10]. Combined information from the fluorescence intensities and lifetimes of NAD(P)H and FAD provide a measure of the global metabolic activity in individual cells within intact samples [3, 7, 10, 13], specifically on redox balance and enzyme binding activity. Previous studies have established that OMI (imaging the fluorescence intensities and lifetimes of NAD(P)H and FAD) is sensitive to cancer progression and drug response [7-9, 28].

The goal of this study is to use OMI to discriminate proliferating, quiescent, and apoptotic cell populations. We hypothesized that populations exhibiting varying cell cycle activity can be

metabolically distinguished upon comparison of fluorescence lifetimes and redox ratio. Here, we demonstrate the feasibility of OMI to identify sub-populations in an acute myeloid leukemia (AML) model, a well-defined model for observing cell cycle status. Pure and heterogeneous populations of each cell type were evaluated using OMI. The results illustrate that OMI can distinguish between proliferating, quiescent, and apoptotic cell populations within a heterogeneous sample. Therefore, OMI could be translated for use in solid tumors to differentiate heterogeneous cancer cell populations within intact samples and *in vivo*, and thus promote a better understanding of the underlying complexity of environmental influence on cancer progression and treatment resistance.

Materials and methods

Cell culture

Kasumi-1 cells (acute myeloid leukemia progenitors) in suspension were cultured in RPMI 1640 medium supplemented with 10% fetal bovine serum and 1% penicillin:streptomycin. Proliferation, quiescence, and apoptosis groups were generated by replacing RPMI media with untreated media or media supplemented with 250nM JQ1 (a transcription inhibitor inducing quiescence [6]), or 2.1 μM cytarabine (Ara-C, standard chemotherapy that induces apoptosis [18]), respectively. Cells were imaged 72 hours after treatment. For imaging, cells were plated onto 35 mm glass bottom dishes (MatTek) and overlaid with a coverslip immediately prior to imaging, at a density of 2.5×10^4 cells per dish.

Cell cycle activity in each culture was validated with flow cytometry. Cells from proliferation, quiescence, and apoptosis groups were seeded at a density of $2.5x10^6$ cells per milliliter in 75-T tissue culture flasks. 72 hours after treatment, each culture was labeled with Ki-67 (proliferation), cleaved caspase 3 (apoptosis), Hoechst 3342 and pyronin Y (quiescence) to confirm cell cycle status of each respective culture via flow cytometry.

Verification of Metabolism with Varied Cell Cycle Status

The dominant role of oxidative phosphorylation in leukemic progenitor cells was confirmed upon perturbation with cyanide. Proliferating Kasumi-1 cells were plated on 35 mm glass dishes at $2.5x10^4$ cells per dish after a 72-hour incubation period. Following acquisition of NAD(P)H and FAD images, cell media was replaced with media supplemented with 4mM NaCN and imaged five minutes after media change.

To verify metabolism associated with an inhibitor-induced quiescent state, cells from the proliferation and quiescence cultures were resuspended in media supplemented with 100 nM of etomoxir, an inhibitor of fatty acid oxidation [19]. Following treatment, cells were incubated for 48 hours and imaged using fluorescence lifetime imaging

Fluorescence Lifetime Imaging

Fluorescence image collection was conducted on a custom-built multi-photon fluorescence microscope. Excitation and emission light through an inverted microscope objective was coupled using a 40X (1.3NA) oil-immersion objective. A titanium:sapphire laser was used for autofluorescence excitation at wavelengths corresponding to NAD(P)H (750 nm) and FAD (890 nm) autofluorescence. A 400-480 nm bandpass filter was used to isolate fluorescence emission for

NAD(P)H. Additionally, combined use of a 500 nm high pass dichroic mirror and a 500-600 nm bandpass filter allow isolation of FAD fluorescence emission. Detection of NAD(P)H and FAD fluorescence emission was possible using a GaAsP photomultiplier tube. Time-correlated single photon counting electronics were used for acquisition of fluorescence lifetime images. Acquistion of 170 x 170 μm (256 x 256 pixels) images required a 60-second integration time and pixel dwell time of 4.8 microseconds. Photobleaching of the sample was avoided during image acquisition by maintaining photon count rates at approximately 1-2 x 10^5 photons/second. NAD(P)H and FAD fluorescence lifetime was measured for each experimental group at 24 and 72 hours following perturbation. Between NAD(P)H and FAD lifetime images in each sample, fields of view were kept consistent.

Image Analysis

Fluorescence lifetime components (SPCImage) were calculated following analysis of fluorescence lifetime images. Fluorescence contributions from background and nuclei of cells was minimized upon application of a threshold value to all images. The measured instrument response function was deconvolved from the decay curve measurement prior to curve fitting. The second harmonic generated signal from urea crystals at 900 nm excitation was used to measure the instrument response function, which was found to have a full width at half maximum of 220 ps. Calculation of fluorescence lifetime values was achieved by fitting decay curves to a two-component exponential model, $I(t) = \alpha_1 e^{-t/\tau1} + \alpha_2 e^{-t/\tau2} + C$, where $I(t)$ is the fluorescence intensity at time t following laser excitation, τ_1 and τ_2 are the short and long fluorescence lifetimes, α_1 and α_2 represent the short and long lifetime component contributions ($\alpha_1 + \alpha_2 = 1$), and C represents background light contribution. A two-component decay curve was used to represent the free and

protein-bound conformations of NAD(P)H and FAD [9]. Photon counts from the NAD(P)H and FAD fluorescence lifetime images were integrated over the fluorescence decay time on a per-pixel basis in order to generate NAD(P)H and FAD intensity images. Respective mean lifetimes of NAD(P)H and FAD were calculated as a weighted average of the short and long lifetimes ($\tau_m = \alpha_1\tau_1 + \alpha_2\tau_2$). Furthermore, computation of redox ratio for each pixel per image was conducted by dividing NAD(P)H fluorescence intensity by FAD fluorescence intensity per pixel. A customized CellProfiler pipeline was used to calculate mean redox ratio values, NAD(P)H and FAD mean lifetimes corresponding to a single image [5]. Fluorescent bead measurements were acquired daily to validate experimental fluorescence lifetime values. Bead lifetime measurements (1.9 ± 0.09 nanoseconds) were consistent with values reported in literature [15, 28].

Partial Least Squares - Discriminant Analysis

In order to obtain maximal separation between groups with differing cell cycle activity, partial least squares discriminant analysis [24] was implemented to build a model determining the contribution of available metabolic measurements to each data set. This technique performs iterations of linear transformations on a matrix of samples with known classification for projection onto a vector comprised of classification values corresponding to each sample in the matrix. The resultant equation represents an optimal boundary between all groups included in model construction. Weight centering of all groups was applied to minimize bias in separation boundaries influenced by uneven cell numbers, by averaging the means across all groups and subtracting the result from each value in the data set. Separate models were developed for two-group and three-group classification to overcome skewed weighting criteria by the training data set. Calculation of

the Mahalanobis distance from each class mean to all data points ensured appropriate assignment of separation boundaries in the case of three-group classification [24].

Acquired images from pure proliferative, quiescent, and apoptotic samples at 72 hours were used as a training set to develop the aforementioned models. In order to validate these models, heterogeneous samples were generated by plating cells from each population at various proportions and imaged immediately following plating. For the two-group validation set, proliferative and quiescent cells were plated at the following proportions: 100:0, 70:30, 50:50, 30:70, 0:100 (proliferating:quiescent). Three- group validation included plating proportions of 33:33:33, 50:25:25, and 25:25:50 (proliferating:quiescent:apoptotic).

Statistical Analysis

To assess significant differences between groups as assessed by the redox ratio, NAD(P)H τ_m and FAD τ_m, a Wilcoxon rank sum test was conducted. For correction of multiple comparisons across data sets, a Tukey multiple comparison test was applied for comparisons of means following multi-group classification. Error bars are representative of the mean ± standard error of the mean. Statistical significance was indicated with an α value less than 0.05.

Results

Metabolic Perturbations in Proliferating and Quiescent Cells

Metabolism of proliferating human acute myeloid leukemia cells was assessed by perturbation with cyanide. Cyanide inhibits oxidative phosphorylation, resulting in an abundance

of NADH in the cytoplasm. The significant increase in the redox ratio after cyanide treatment (Fig. 1A) confirms the reported dominance of oxidative phosphorylation in leukemic cells. Similarly, the reduced NADH τ_m is consistent with previous studies of cyanide treatment in cancer cells (Fig. 1B) [refs]. Trends in FAD τ_m were also comparable to previously reported data, however there was not a significant change in the FAD τ_m following addition of cyanide.

Unlike proliferating leukemic cells, quiescent leukemic cells are known to rely on fatty acid oxidation, which is a feeder reaction for oxidative phosphorylation [18, 19]. JQ1 is also known to induce quiescence in leukemic cells [6]. In order to validate the effect of JQ1, leukemic cells were treated with the fatty acid oxidation inhibitor etomoxir [19] (Fig. 2). As expected, inhibition of fatty acid oxidation did not result in significant changes in the redox ratio of proliferating cells (Fig. 2A). However, inhibition of fatty acid oxidation did increase the redox ratio of quiescent cells (Fig. 2A). These results verify that JQ1 induces these leukemic cells into quiescence, which is characterized by the reliance on fatty acid oxidation.
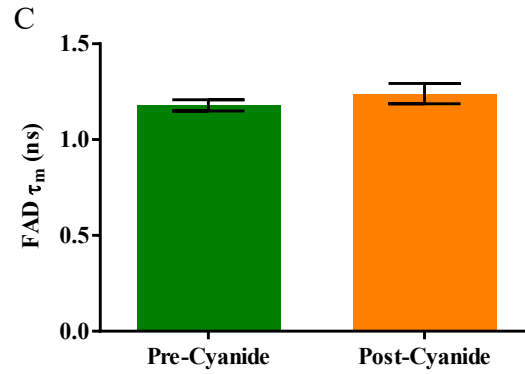

15
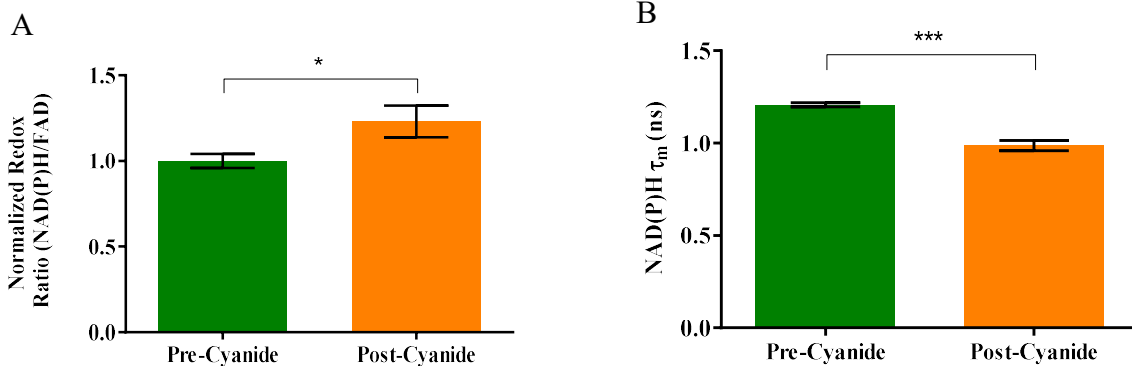
Figure 1. Inhibition of Oxidative Phosphorylation. Quantitative measurement (mean +/- SE) of the (A) redox ratio, (B) NAD(P)H mean lifetime (τ_m), and (C) FAD τ_m for proliferating Kasumi-1 cells (n = 8) before and five minutes after addition of 4 mM cyanide. Redox ratio values increased with addition of cyanide, indicating inhibition of oxidative phosphorylation (* p<0.05, *** p < 0.001)
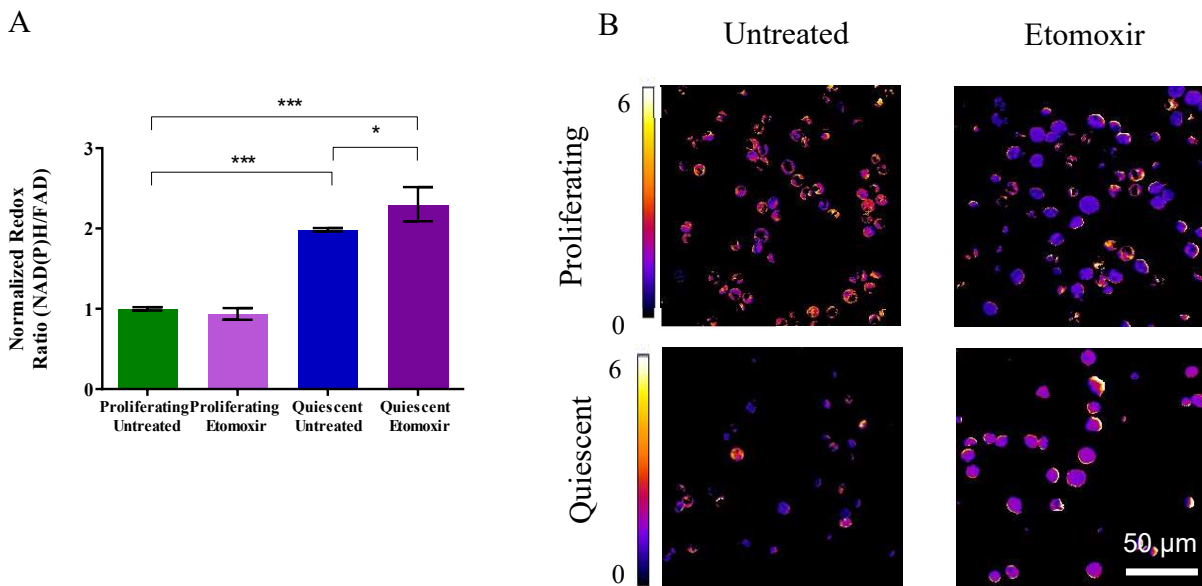

Figure 2. Inhibition of Fatty Acid Oxidation. (A) Quantitative measurement (mean +/- SE) of the redox ratio for untreated proliferating (n =12 images) and quiescent (n= 12 image) Kasumi-1 cells, as well as etomoxir-treated proliferating (n =12 images) and quiescent (n =12 images) cells. Kasumi-1 cells were forced into quiescence by treatment with 250 nM JQ1 72 hours before etomoxir or vehicle treatment. (B) Representative redox ratio images. The increase in the redox ratio after etomoxir treatment indicate that inhibition of fatty acid oxidation also inhibits downstream oxidative phosphorylation in quiescent cells only. (* p<0.05, *** p < 0.001)

<u>OMI of Proliferative, Quiescent, and Apoptotic Cells</u>

OMI was performed in acute myeloid leukemia cells forced into proliferative, apoptotic, and

quiescent states, in order to validate OMI as a method for classifying these cell states.   Gold

standard flow cytometry verified cell cycle activity associated with each population. Untreated

(proliferative), JQ1-treated (quiescent), and cytarabine-treated (apoptotic) Kasumi-1 cells were

treated and imaged at 24 and 72 hours post-treatment. Two-photon fluorescence lifetime imaging

quantified the redox ratio, NAD(P)H τ_m, and FAD τ_m within proliferating, quiescent, and

apoptotic cell populations (Fig. 3). The redox ratio progressively increases for apoptotic and

quiescent cells compared to proliferative cells ($p < 0.05$, Fig. 3A). The NAD(P)H τ_m increases for

apoptotic cells compared to proliferative and quiescent cells ($p < 0.05$, Fig. 3B). The FAD τ_m is

greater for apoptotic and quiescent cells compared to proliferating cells ($p < 0.05$, Fig. 3C).

Furthermore, cellular morphology can also discriminate between cells with varied cell cycle

status. Quiescent cells exhibit a decrease in cytoplasmic area (Fig. 4) compared to proliferative

and apoptotic populations ($p < 0.05$, data not shown), undergoing size reduction at later time

points. Subpopulation distributions exhibited large overlap for single-cell redox ratio values.

This trend was similarly observed across mean NAD(P)H and FAD lifetimes, indicating that

individual metabolic measurements provide limited separation between subpopulations.

However, the previously-observed differences in mean values of each metabolic measurement

suggests that a combination of these parameters could allow for identification of cell cycle

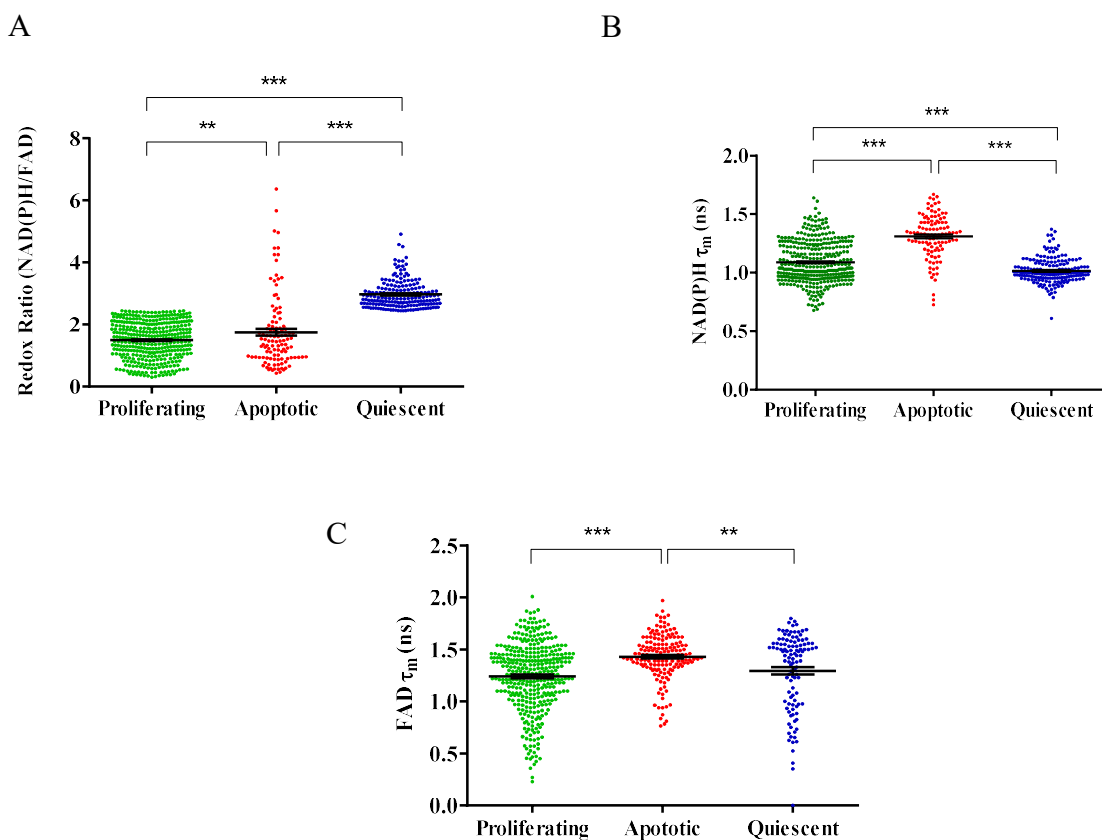activity on a cell-by-cell basis.

17

Figure 3. Metabolic Measurements of Proliferating, Apoptotic, and Quiescent Cells. Quantitative measurement (mean +/- SE) of the (A) redox ratio, (B) NAD(P)H τ_m, and (C) FAD τ_m at the single-cell level for proliferating (n = 12 images), quiescent (n = 12 images), and apoptotic (n = 12 images) Kasumi-1 cells at 72 hours post-treatment. Significant differences were observed in redox ratio and lifetime values across all populations (* $p < 0.05$, ** $p < 0.01$, *** $p < 0.001$). Individual metabolic measurements provide limited separation between subpopulations.
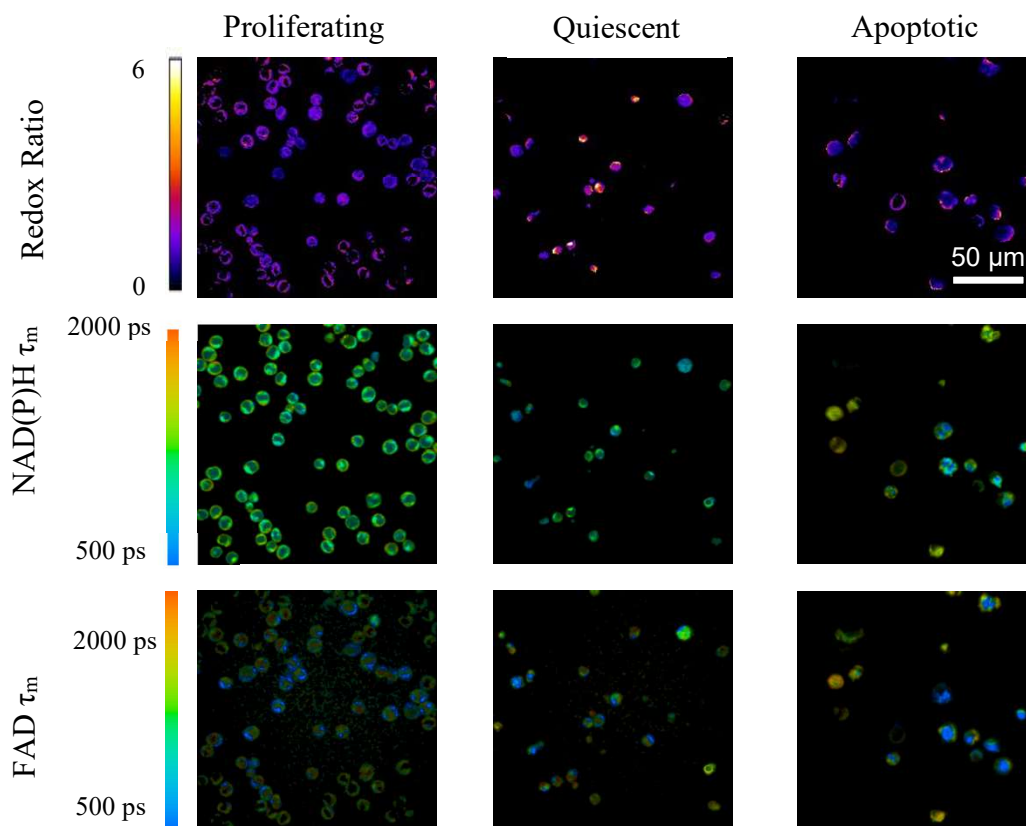
Figure 4. Lifetime and redox images. Representative redox ratio, NAD(P)H τ_m, and FAD τ_m images of Kasumi-1 cells forced into proliferative, quiescent, and apoptotic states, 72 hours post-treatment.

Classification Model with Partial Least Squares – Discriminant Analysis (PLS-DA)

In order to enhance discrimination between cell cycle status on the single-cell level, partial least squares – discriminant analysis (PLS-DA) was performed to maximize separation between each population. The first iteration of the PLS-DA model aims to separate proliferating and quiescent cell populations. The two-group PLS-DA model provided a linear combination of the measured metabolic parameters (redox ratio, NAD(P)H τ_m, FAD τ_m), weighted based on their significance in representing training set data, for separation between proliferating and quiescent

cultures. This two-group PLS-DA model was applied to an initial training data set, consisting of

measurements from pure samples of quiescent and proliferative cells (Fig. 5A). The two-group

PLS-DA model showed improved separation of proliferating and quiescent populations (Fig. 5A)

compared to any single variable (Fig. 3). This approach was extended to include all three

populations, again using measurements of pure samples from quiescent, proliferative, and

apoptotic cells for the initial training data set (Fig. 5B). Again, the three-group PLS-DA model

showed improved separation of proliferating, quiescent, and apoptotic populations (Fig. 5B)
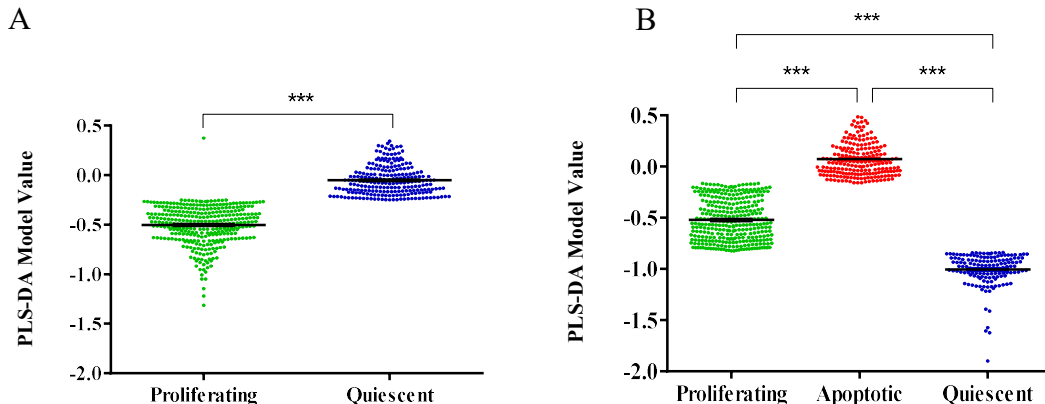
compared to any single variable (Fig. 3).

Figure 5. Two– and Three– Group PLS-DA Model Training Sets. Quantitative measurement (mean +/- SE) of values determined from a PLS-DA model. (A) Single-cell population distributions from the PLS-DA model applied to a two-group training set (proliferating: n = 12 images, quiescent: n = 12 images) (B) Single-cell population distributions from the PLS-DA model applied to a three-group training set (proliferating: n = 12 images, quiescent: n = 12 images, apoptotic: n = 12 images). The PLS-DA model results in significant improvement in separation between populations (*** p < 0.001) compared to any single variable alone (Fig. 3).

Validation of the Two- and Three-Group PLS-DA Models

The two- and three-group PLS-DA models were validated on heterogeneous, mixed

cultures of proliferative, quiescent, and apoptotic cells. The two-group model was validated with

images of proliferating and quiescent cell mixtures plated at varied proportions (100:0, 70:30,

50:50, 30:70, 0:100, respectively), to evaluate the ability of the model to distinguish both subpopulations in a single sample (Fig. 6). The two-group PLS-DA model classified proliferative cells and quiescent cells with high accuracy, based on the gold standard plated ratio (Table 1).
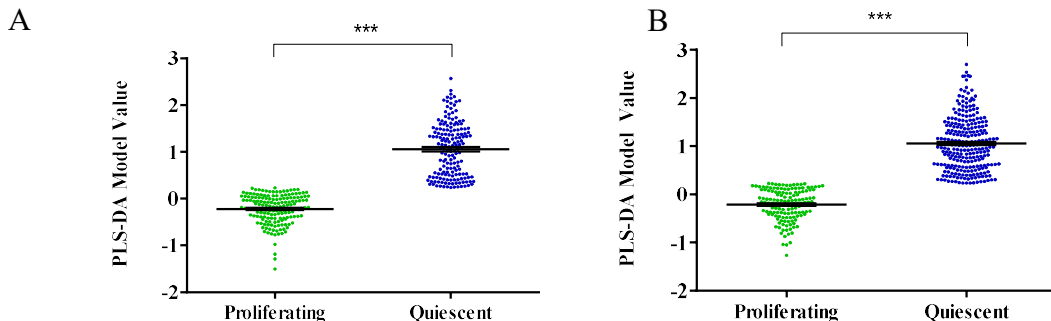

Figure 6. Two-Group PLS-DA Model Validation. Quantitative measurement (mean +/- SE) of values determined from a two-group PLS-DA model. (A) Single-cell population distributions from PLS-DA model applied to a validation set with equal proportions of plated proliferating and quiescent cells (n = 12 images) (B) Single-cell population distributions from the PLS-DA model applied to a validation set plated at a proportion 70% proliferating and 30% quiescent cells (n = 12 images). The two-group PLS-DA model results in high classification accuracy compared to plated proportions (*** p < 0.001).

Table 1: Comparison of Plated and Modeled Proportions for Two-Group Mixtures

Proliferating:Quiescent	Mixture 1	Mixture 2
Plated Proportions	50 : 50	30 : 70
Model Proportions	50 : 50	36 : 64

Similarly, the three-group model was evaluated on mixtures of all populations plated at the following ratios: 33:33:33, 50:25:25, 25:25:50 (proliferating, quiescent, apoptotic), to observe population-dominant changes in sensitivity to quiescent populations (Fig. 7B). The three-group

21

model resulted in high classification accuracy for all three populations in mixed samples with equal

proportions of cells from each population (Table 1). Similar trends were observed in proliferation-

dominant samples, with minimal decrease in sensitivity. Apoptotic-dominant samples, however,

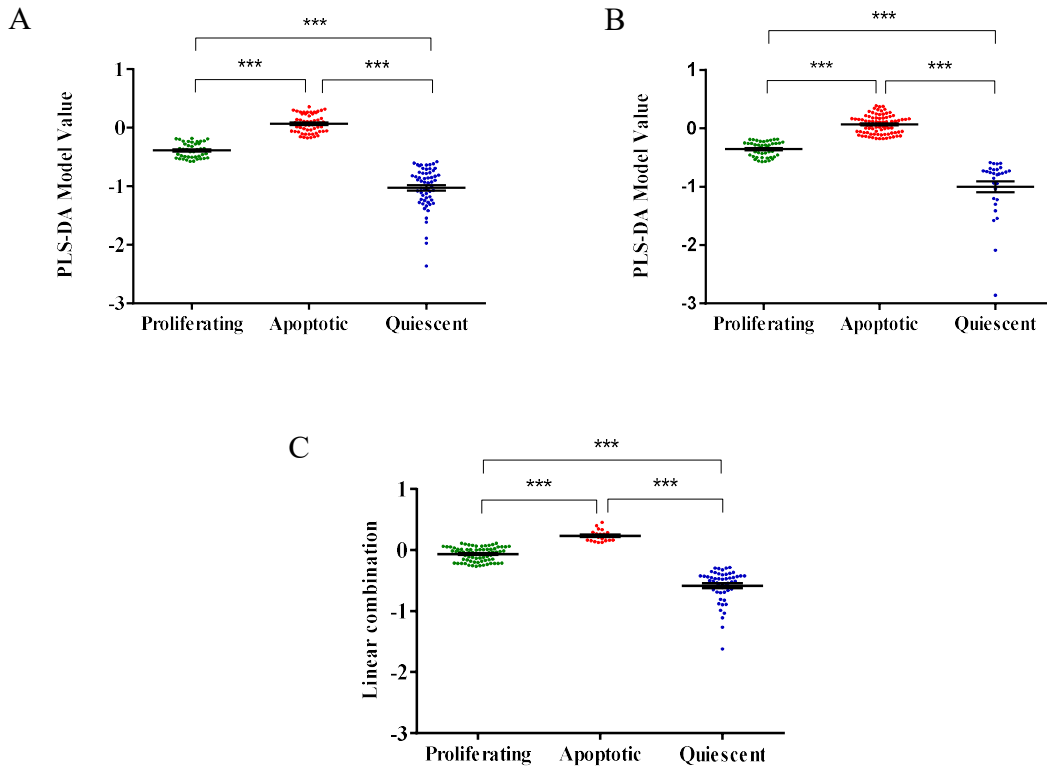introduced challenges in distinguishing between apoptotic and quiescent cells.

Figure 7. Three-Group PLS-DA Model Validation. Quantitative measurement (mean +/- SE) of values determined from a three-group PLS-DA model. (A) Single-cell population distributions from PLS-DA model applied to a validation set with equal proportions of plated proliferating, apoptotic, and quiescent cells (n = 12 images) (B) Single-cell population distributions from PLS-DA model applied to a validation set plated at a proportion of 25% proliferating, 50% apoptotic, and 25% quiescent cells (n = 12 images). (C) Single-cell population distributions from PLS-DA model applied to a validation set plated at a proportion of 50% proliferating, 25% apoptotic, and 25% quiescent cells (n = 12 images). The three-group PLS-DA model similarly results in high classification accuracy compared to plated proportions (*** p < 0.001).

Table 2: Comparison of Plated and Modeled Proportions for Three-Group Mixtures

Proliferating:Apoptotic:Quiescent	Mixture 1: Equal proportions	Mixture 2: Apoptotic dominant	Mixture 3: Proliferating dominant
Plated Proportions	33 : 33 : 33	25 : 50 : 25	50 : 25 : 25
Model Proportions	36 : 26 : 37	28 : 53 : 19	50 : 14 : 36

Discussion

Tumor heterogeneity is a significant challenge in new drug development and treatment planning in cancer [1]. Unfortunately, there are a lack of methods to assess tumor heterogeneity without the use of contrast agents in intact samples. Metabolism is an attractive measure of tumor heterogeneity, due to its fundamental role in malignant transformation and in drug resistance [1-3]. Our results demonstrate that OMI can discriminate between populations exhibiting heterogeneous cell cycle activity in a single sample, without the use of contrast agents. OMI has been previously used to study single-cell response *in vivo* [3, 7, 28] and in three-dimensional cultures [15]. These studies further support the use of OMI to identify and characterize sources of tumor heterogeneity in these samples. Therefore, the current study provides a framework to understand the metabolic sources of tumor heterogeneity in relevant samples, thus providing further insight into strategies to circumvent drug resistance.

To our knowledge, this study is the first to classify cell populations based on cell-cycle associated differences in metabolism. However, previous studies have characterized the metabolism of leukemic cells in different cell cycle phases. Lagadinou et al. identified oxidative phosphorylation as the primary energy source for leukemic progenitor cells, by observing levels of reactive oxygen species produced by these cells [18]. These findings are consistent with our studies, specifically with the increased redox ratio in Kasumi-1 cells upon inhibition of oxidative

phosphorylation with cyanide (p < 0.05, Fig. 1). Oxidative phosphorylation is driven by metabolites produced in upstream pathways, which promote these cells to adopt different functional phenotypes. Samudio et al. similarly characterized the oxygen consumption of leukemia progenitors in proliferative or quiescent states [19]. These studies showed that proliferative leukemic cells use more glycolytic metabolism compared to quiescent cells. Furthermore, perturbation with a fatty acid oxidation inhibitor (etomoxir) eradicated the quiescent cells [19], suggesting these cells rely on fatty acid oxidation to drive oxidative phosphorylation downstream. Our results with the same fatty acid oxidation inhibitor (Fig. 2) are consistent with these previous findings [19], and validate the reliance of quiescent leukemic cells on fatty acid oxidation (in contrast to proliferative leukemic cells). Additionally, comparison of redox ratio, NAD(P)H τ_m and FAD τ_m across proliferative, apoptotic, and quiescent cells indicate that variations in metabolism are required for differences in functional phenotype (Fig. 3).

The original OMI variables (redox ratio, NAD(P)H τ_m, FAD τ_m) are somewhat effective in distinguishing proliferative, apoptotic, and quiescent cells *in vitro* (Fig. 3). To optimize single-cell classification, we applied PLS-DA to generate a linear combination model of the measured OMI variables. Our results show that this PLS-DA model improves the separation of proliferative, quiescent, and apoptotic cells in a pure sample (training set, Fig. 5) and in heterogeneous samples (validation sets, Figs. 6,7). Agreement between the plated proportions and the PLS-DA model-predicted proportions are good for both the two-group (Table 1) and three-group (Table 2) models. Single cell tracking studies could provide further evaluation of the correlation between plated and PLS-DA model cell classifications. These results suggest that OMI combined with a PLS-DA model can identify proliferative, apoptotic, and quiescent cells in unknown, heterogeneous samples. This could be a powerful tool to observe the interactions of these cells within tumors.

The results of this study have potential for contributing to studies of tumor dormancy and drug resistance. Tumor dormancy has been identified as a primary source of resistance to conventional therapies, with the inactive nature of the tumor resulting in a lack of treatment response [1, 17]. There are many theories on the mechanisms driving tumor dormancy. One predominant theory suggests that, at the single-cell level, quiescence within the tumor promotes the bulk mass to enter a state of dormancy [17, 25-27]. The OMI and PLS-DA approach used in this paper to identify and monitor quiescent tumor cells in the presence of both proliferative and apoptotic cells could be used to study interactions between cell types, and the effect of quiescence on tumor progression. Our findings could also be used to identify extracellular influences that initiate transitions between quiescence, proliferation, and apoptosis. Furthermore, these results support the use of cellular metabolic measurements to study the development of tumor dormancy.

Additional studies will be necessary to evaluate our approach to universally examine cell cycle-driven tumor heterogeneity. Since transition between proliferation, quiescence, and apoptosis is largely controlled by changes in cellular metabolism, metabolic analysis of these sub-populations should correlate to underlying mechanisms driving functional activity of multiple cancer cell types. Translation to *in vivo* cancer models, such as breast or pancreatic cancer, should be possible upon characterization of metabolic differences associated with cell cycle status in these cell types. Moreover, transition to three-dimensional organotypic cultures or *in vivo* mouse studies would provide spatial relationships between quiescent cells and other cell types, as well as provide more relevant information in understanding the role of tumor heterogeneity in patient treatment resistance. Overall, we have demonstrated OMI and PLS-DA as valuable tools for observing cell-

cycle status. Ultimately, these tools can be used to better understand tumor dormancy and treatment resistance.

Chapter III

CONCLUSION AND FUTURE DIRECTIONS

Differences in metabolic activity were observed between populations of proliferating, quiescent, and apoptotic cells in a well-defined acute myeloid leukemia model, exhibiting the sensitivity of optical metabolic imaging to cell cycle activity. Upon treatment of leukemic cells with perturbations inducing each of the aforementioned functional states, significant differences were detected in redox ratio and fluorescence lifetimes of NADH and FAD across all populations. This finding supports reported trends in literature characterizing the oxidative metabolism of proliferating and quiescent leukemic cells driven by glycolysis and fatty acid oxidation, respectively. Furthermore, application of the classification model developed in this study demonstrated the ability to distinguish each cell type within a mixed sample. These results suggest that optical metabolic imaging could serve as a tool to identify and characterize heterogeneous populations in tumor samples to study their contribution to treatment resistance.

Additional studies are required to establish the feasibility of identifying these populations in three-dimensional culture or *in vivo*. Metabolic characterization and classification of these cell populations within three-dimensional cultures or *in vivo* in mice will be necessary to verify the sensitivity and universal applicability of this technique. Following appropriate validation, this technique could establish a platform for studying the influence of tumor microenvironment on tumor cell dormancy.

REFERENCES

1. Junttila MR, De sauvage FJ. Influence of tumour micro-environment heterogeneity on therapeutic response. Nature. 2013;501(7467):346-54.

2. Ganeshan K, Chawla A. Metabolic regulation of immune responses. Annu Rev Immunol. 2014;32:609-34.

3. Georgakoudi I, Quinn KP. Optical imaging using endogenous contrast to assess metabolic state. Annu Rev Biomed Eng. 2012;14:351-67.

4. Lakowicz JR, Szmacinski H, Nowaczyk K, Johnson ML. Fluorescence lifetime imaging of free and protein-bound NADH. Proc Natl Acad Sci USA. 1992;89(4):1271-5.

5. Walsh AJ, Skala, MC. An automated image processing routine for segmentation of cell cytoplasms in high-resolution autofluorescence images. SPIE Proceedings. 2014; 8948

6. Filippakopoulos P, Qi J, Picaud S, et al. Selective inhibition of BET bromodomains. Nature. 2010;468(7327):1067-73.

7. Skala MC, Riching KM, Gendron-fitzpatrick A, et al. In vivo multiphoton microscopy of NADH and FAD redox states, fluorescence lifetimes, and cellular morphology in precancerous epithelia. Proc Natl Acad Sci USA. 2007;104(49):19494-9.

8. Walsh A, Cook RS, Rexer B, Arteaga CL, Skala MC. Optical imaging of metabolism in HER2 overexpressing breast cancer cells. Biomed Opt Express. 2012;3(1):75-85.

9. Walsh AJ, Poole KM, Duvall CL, Skala MC. Ex vivo optical metabolic measurements from cultured tissue reflect in vivo tissue status. J Biomed Opt. 2012;17(11):116015.

10. Conklin MW, Provenzano PP, Eliceiri KW, Sullivan R, Keely PJ. Fluorescence lifetime imaging of endogenous fluorophores in histopathology sections reveals differences between normal and tumor epithelium in carcinoma in situ of the breast. Cell Biochem Biophys. 2009;53(3):145-57.

11. Eto K, Tsubamoto Y, Terauchi Y, et al. Role of NADH shuttle system in glucose-induced activation of mitochondrial metabolism and insulin secretion. Science. 1999;283(5404):981-5.

12. Heikal AA. Intracellular coenzymes as natural biomarkers for metabolic activities and mitochondrial anomalies. Biomark Med. 2010;4(2):241-63.

13. Chance B, Legallais V, Schoener B. Metabolically linked changes in fluorescence emission spectra of cortex of rat brain, kidney and adrenal gland. Nature. 1962;195:1073-5.

14. Mayevsky A. Mitochondrial function and energy metabolism in cancer cells: past overview and future perspectives. Mitochondrion. 2009;9(3):165-79.

15. Walsh AJ, Cook RS, Sanders ME, et al. Quantitative optical imaging of primary tumor organoid metabolism predicts drug response in breast cancer. Cancer Res. 2014;74(18):5184-94.

16. Cai L, Tu BP. Driving the cell cycle through metabolism. Annu Rev Cell Dev Biol. 2012;28:59-87.

17. Saudemont A, Quesnel B. In a model of tumor dormancy, long-term persistent leukemic cells have increased B7-H1 and B7.1 expression and resist CTL-mediated lysis. Blood. 2004;104(7):2124-33.

18. Lagadinou ED, Sach A, Callahan K, et al. BCL-2 inhibition targets oxidative phosphorylation and selectively eradicates quiescent human leukemia stem cells. Cell Stem Cell. 2013;12(3):329-41.

19. Samudio I, Harmancey R, Fiegl M, et al. Pharmacologic inhibition of fatty acid oxidation sensitizes human leukemia cells to apoptosis induction. J Clin Invest. 2010;120(1):142-56.

20. Varone A, Xylas J, Quinn KP, et al. Endogenous two-photon fluorescence imaging elucidates metabolic changes related to enhanced glycolysis and glutamine consumption in precancerous epithelial tissues. Cancer Res. 2014;74(11):3067-75.

21. Nakashima N, et al. J Biol Chem. 1980;255(11):5261-3.

22. Blacker TS, Mann ZF, Gale JE, et al. Separating NADH and NADPH fluorescence in live cells and tissues using FLIM. Nat Commun. 2014;5:3936.

23. Konig K, et al. J Biomed Opt. 2003; 8:432–439.

24. Brereton RG, Lloyd GR. Partial least squares discriminant analysis: taking the magic away, J Chemometrics. 2014; 28:213-225.

25. Sosa MS, Bragado P, Aguirre-ghiso JA. Mechanisms of disseminated cancer cell dormancy: an awakening field. Nat Rev Cancer. 2014;14(9):611-22.Sosa et al Nat reviews 2014 vol 14 611-622

26. Bragado P, Sosa MS, Keely P, Condeelis J, Aguirre-ghiso JA. Microenvironments dictating tumor cell dormancy. Recent Results Cancer Res. 2012;195:25-39.

27. Baxevanis CN, Perez SA. Cancer Dormancy: A Regulatory Role for Endogenous Immunity in Establishing and Maintaining the Tumor Dormant State. Vaccines (Basel). 2015;3(3):597-619.

28. Walsh AJ, Cook RS, Manning HC, et al. Optical metabolic imaging identifies glycolytic levels, subtypes, and early-treatment response in breast cancer. Cancer Res. 2013;73(20):6164-74.